NANO EXPRESS

Thermal Evaporation Synthesis and Properties of ZnO Nano/Microstructures Using Carbon Group Elements as the Reducing Agents

H. Lv · D. D. Sang · H. D. Li · X. B. Du · D. M. Li · G. T. Zou

Abstract ZnO nano/microstructures have been formed by thermal evaporation method using ZnO powders mixed with carbon group elements (C, Si, Ge, Sn, or Pb) as the reducing agent. For cases of mixed precursors of ZnO/C, ZnO/Si, and ZnO/Ge, the pure ZnO nano/microstructures are realized, while for ZnO/Sn (ZnO/Pb) systems, the phase of Pb_2O_3 (Zn_2SnO_4) generally are represented in the ZnO products. The appearance of Pb_2O_3 (Zn_2SnO_4) is attributed to the lower melting point and higher vapor pressure of Sn (Pb) in the heating and evaporation processes. The morphologies and sizes of the products are controlled by adjusting the growth regions and/or introducing gaseous argon. Room temperature (RT) photoluminescence spectra indicate that the intensity (peak position) of the ultraviolet emission is increased (redshift) due to the existence of Zn_2SnO_4 phase in the ZnO products. The Pb_2O_3 (Zn_2SnO_4) phase in ZnO nano/microstructures plays a important role in enhancing the saturation magnetizations of RT ferromagnetism with respect to the case of pure ZnO products fabricated by the precursor of mixed ZnO and graphite.

Keywords ZnO nano/microstructures · Thermal evaporation · Reducing agents of carbon group elements · Growth mechanism · Optical and ferromagnetic properties

H. Lv · D. D. Sang · H. D. Li (✉) · D. M. Li · G. T. Zou
State Key Laboratory of Superhard Materials, Jilin University, 130012 Changchun, China
e-mail: hdli@jlu.edu.cn

X. B. Du
College of Physics, Jilin University, 130012 Changchun, China

Introduction

In recent decades, great interests have been focused on zinc oxide (ZnO) since it has a wide band gap and large exciton binding energy. ZnO nano/microstructures have led to some important applications, for example, in the fields of UV laser with low threshold [1, 2], field emission array [3, 4], surface acoustic wave device [5], transistor,[6] and biosensor [7, 8]. For the synthesis of ZnO nanostructures, thermal evaporation method has been widely used. The reducing agent of graphite was generally mixed with ZnO powder to fabricate pure nanostructural ZnO at a temperature of 1,000–1,100 °C [9, 10]. Due to the introduction of carbon, ZnO precursor (melting point: 1,975 °C) is reduced and the Zn and ZnO_x (evaporated at <500 °C) are formed, which subsequently combined with oxygen to synthesize ZnO products. Recently, our group [11] reported that besides the conventional graphite, a variety of metallic elements can be used as the effective reducing agent to achieve pure ZnO nano/microstructures by the thermal evaporation method. It speculates that the elements in the periodic table that have relatively small ionization energy can be used as new reducing agents. It is therefore essential to thoroughly understand the more new reducing agents to extend the researches on numerous fabrication and application of ZnO.

In this paper, we systemically study the synthesizing ZnO nano/microstructures using carbon group elements, i.e., graphite-C, silicon-Si, germanium-Ge, tin-Sn, and plumbum-Pb as the reducing agent. The heating temperatures (T_{heat}, the critical temperature for thermal reducing and vaporizing the source) for the sources of ZnO–Si, –Ge, –Sn and –Pb systems are lower than the conventional graphite, which is related to the strong reducibility of these new additions. It is found that due to the more activity of

Sn and Pb than C, Si, and Ge, the oxides of Sn and Pb appear in the corresponding products. The growth mechanism and optical and magnetic properties of the samples are investigated.

Experiments

The experiments were carried out in a horizontal tube furnace under atmospheric pressure. To further study the growth behaviors of the products, the growth with and without introducing gaseous argon (Ar) were proposed. Mixed ZnO and the reducing agent (graphite, Si, Ge, Sn, or Pb) powders (mass ratio: 1:1) were placed at the end of a slender one-end sealed quartz tube. After the furnace was heated up to the setting temperature (T_{heat}), the quartz tube with raw materials was inserted into the furnace. Si strips were used as the substrates and placed downstream from the source to the open end of the tube at relatively low temperatures (estimated based on a carefully calibrated temperature gradient by a thermocouple). After growth for 1.5–2 h, the samples were drawn out and cooled to room temperature (RT).

The series of experiments were performed for various mixed powder precursors (i.e., ZnO-graphite, ZnO–Si, ZnO–Ge, ZnO–Sn, and ZnO–Pb) at their corresponding T_{heat} of 1,100, 850, 700, 800, and 800 °C, respectively. In the experiments, we examined the variation of morphologies and sizes of the products grown at different growth temperatures (T_{growth}) and with (without) introducing gaseous Ar.

The crystal structures of the products were investigated by X-ray diffraction (XRD, Rigaku D/max-rA, with Cu Kα radiation). The morphology and composition of the products were characterized using scanning SEM (JSM-6480LV) equipped with electron energy-dispersive X-ray

(EDX). Raman scattering spectra were measured by a Renishaw inVia Raman microscope with an argon laser (λ, 514.5 nm) excitation. PL measurements were carried out excited by a 325 nm line of He–Cd laser. Magnetic hysteresis loops of the samples were measured using vibrating sample magnetometer (VSM, LakeShore Model 7410) with the maximum field of 28 kOe. The above examinations were all performed at RT.

Results and Discussions

The morphologies of the samples synthesized by the sources of ZnO mixed with group-IV elements observed by SEM are shown in Fig. 1. In our previous work [11], the cases of reducing agents of Si and Ge have been discussed. The morphologies and compositions of the products synthesized by ZnO–Sn (Fig. 1a–c) and ZnO–Pb (Fig. 1d–f) are studied in detail by SEM (EDX, the inset of Fig. 1) in this letter. In Fig. 1a, micron-sized rods and spheres grown at 750 °C, near the reaction source, are represented. EDX spectrum shows that the sample consists of ZnO, and Sn signal is presented. As discussed later, the signal of Sn originates from the formed Zn_2SnO_4. Collected near the open end of the tube at a relative low temperature of 600 °C without and with introducing gaseous Ar, the diameters of the rods are decreased (Fig. 1b, c). Furthermore, no signals of Sn are found in the EDX spectra for the ZnO products. In Fig. 1d, the wires synthesized are of 300–500 nm in diameter, and under these wires, film-like structures are represented (Fig. 1e), which is a Pb_2O_3 layer determined by EDX. Note that the products are generally several hundreds in diameter synthesized in the atmosphere ambient (Fig. 1a, b, d). By introducing gaseous Ar at a flow rate of 400 sccm in the furnace, the average diameter of the nanorods and/or nanowires, synthesized either by the

Fig. 1 SEM images of ZnO products synthesized by the source of ZnO powder mixed with Sn (**a**–**c**), and Pb (**d**–**f**). The *insets* show the corresponding EDX spectra (The signals of Si originate from Si substrate)
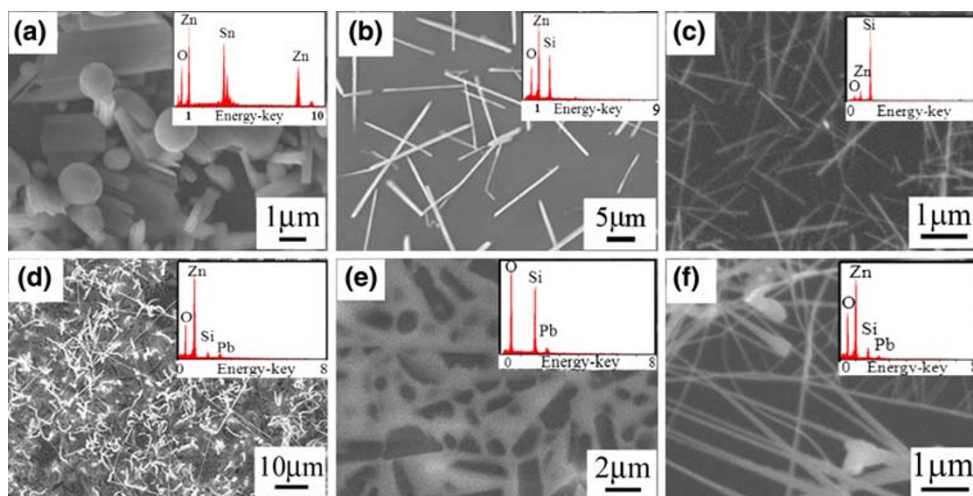
source of ZnO–Sn or ZnO–Pb, are significantly decreased to 50–100 nm, as shown in Fig. 1c and f.

Figure 2a–e shows the typical XRD patterns of the as-prepared samples fabricated from the sources of ZnO-graphite, ZnO–Si, ZnO–Ge, ZnO–Sn, and ZnO–Pb, respectively. For these samples, the main diffraction peaks can be indexed to the hexagonal wurtzite ZnO (JCPDS 79-0206). Pure ZnO nano/microstructures are fabricated from the sources of ZnO-graphite, ZnO–Si, and ZnO–Ge. Importantly, as shown in Fig. 2d and e, it is found that the peaks assigned to Zn_2SnO_4 (JCPDS 04-0736) and Pb_2O_3 (JCPDS 76-1791) appear in the samples using ZnO–Sn and ZnO–Pb as the reaction sources, respectively. The XRD results are consistent with the corresponding EDX spectra. Figure 3a, b, and c shows the Raman spectra of the products formed by the reducing agents of graphite, Si, and Ge. The peaks at 437 and 581 cm^{-1} are attributed to E_{2H}, and E_{1L} of the bulk ZnO mode, respectively [12–14]. According to the results of XRD, SEM (including EDX), and Raman spectra, it is demonstrated that in these cases, pure ZnO nano/microstructures can be realized.

The Raman spectra taken from samples, synthesized by the precursor of ZnO–Sn, collected close to the open end of the tube at a T_{growth} of 600 °C and near the source at 750 °C are shown in Fig. 3d and e. For the former sample (Fig. 3d), pure ZnO can be obtained, as its spectrum shows E_{2H} mode of ZnO. However, for the latter sample (Fig. 3e), a peak at 668 cm^{-1}, which is assigned to the well-known peak of Zn_2SnO_4 [15], is presented in addition to the E_{2H} mode of ZnO, which means that Zn_2SnO_4 appears in the sample. Combining the results of Raman spectra, XRD, and EDX, it is demonstrated that the composition and structure of the samples vary at different growth positions, where the T_{growth} and vaporized sources are different. Figure 3f shows the Raman spectrum of the product
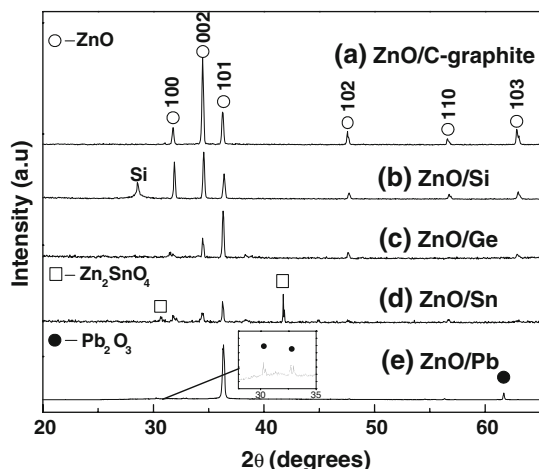

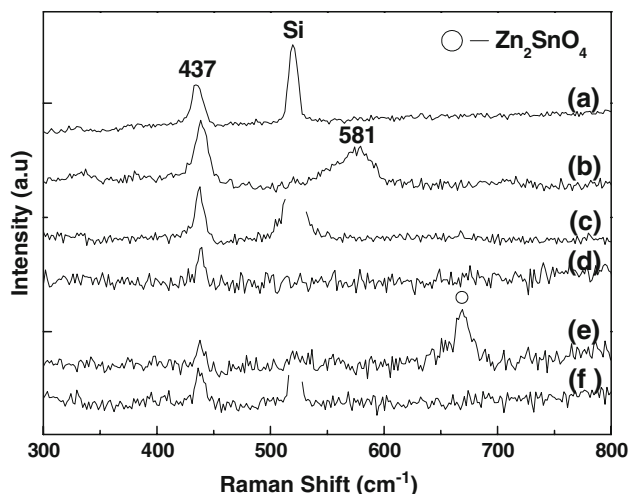**Fig. 2** XRD patterns of the samples synthesized by the source of ZnO powder mixed with graphite (**a**), Si (**b**), Ge (**c**), Sn (**d**), Pb (**e**)

Fig. 3 Raman spectra of the ZnO products synthesized by the source of ZnO powder mixed with graphite (**a**), Si (**b**), Ge (**c**), Sn (**d**, **e**), Pb (**f**). The signals of Si originate from Si substrate

formed by the reaction source of ZnO–Pb. The E_{2H} mode of ZnO is presented; however, no signals from Pb_2O_3 are found in contrast to the observations in the corresponding XRD and EDX spectra. On the one hand, the content of Pb_2O_3 in the product is small to be hardly observed in Raman spectrum, and on the other hand, Raman signals excited by laser beam with small spot size (~ 1 μm) are weaker with respect to XRD spectroscopy that performed for the whole sample.

Generally, for ZnO nanostructures fabricated from the precursor of mixed ZnO and graphite, the reaction temperature was as high as 1,000–1,100 °C. When the reducing agent (A) of Si, Ge, Sn, or Pb replaces graphite, it speculates that main reactions occur as follows:

$$ZnO + A \rightarrow AO + Zn \tag{1}$$

$$ZnO + A \rightarrow AO + ZnO_x \tag{2}$$

The processes are similar to the cases using graphite as the reducing agent [10, 16]. The melting temperature of Zn and ZnO_x is ~ 419 °C (where $x < 1$), which is much lower than that of ZnO (1,975 °C) [17]. The vaporized Zn and Zn suboxide are ideal nuclei for the formation of ZnO nano/microstructures condensed on the substrate. In our experiments, since no particles are found at the ends of ZnO rods observed in SEM images, it is proposed that the growth of the ZnO products follows the vapor–solid (VS) mechanism [10]. For comparison, the intrinsic properties of the carbon group elements (graphite, Si, Ge, Sn, and Pb) and the corresponding T_{heat} are summarized in Table 1. In our previous work [11], it has been demonstrated that the lower characteristic ionization energy of the reducing agents leads to the lower T_{heat} for thermal evaporation processes. Therefore, the data of T_{heat} for the cases of Si, Ge, Sn, and Pb are significantly lower than that of graphite.

Table 1 T_{heat} and intrinsic properties of the carbon group elements for synthesizing ZnO nano/microstructures

| Reducing agent	T_{heat} (°C)	IE = (IE$_1$ + IE$_2$; kJ mol^{-1})	Vapor pressure (torr)[a]	Melting point (°C)
Graphite	1,000	3,439		3,652
Si	850	2,364	4.0×10^{-11}	1,410
Ge	700	2,299	2.0×10^{-11}	937
Sn	800	2,219	7.1×10^{-7}	231
Pb	800	2,165	5.0×10^{-2}	328

[a] Reference [20]

As reported in previous literature, impurity of Sn [18, 19] was intentionally doped in the ZnO nanostructure products synthesized by adding SnO_2 in the mixed powders of ZnO and graphite heated at high temperature of 1,100 °C. In our cases of the precursor of ZnO–Sn or ZnO–Pb heating at a low T_{heat} of about 800 °C, there are a number of Zn_2SnO_4 and Pb_2O_3 appearing in the final ZnO products, as demonstrated by XRD, EDX, and Raman spectral characterizations. This can be attributed to the facts that the melting points (vapor pressures [20] at T_{heat}) of Sn and Pb are significantly lower (higher) than that of graphite, Si, and Ge, as listed in Table 1. Besides Eqs. 1 and 2, SnO_x or PbO_x were also derived from Sn or Pb vapor (by A + $O_2 \rightarrow AO_x$, $x < 1$). After the reduction–oxidation reactions between ZnO and SnO_x (PbO_x), SnO_2 or Pb_2O_3 was formed. Note that for the case of ZnO–Pb (as shown in Fig. 1d and e), ZnO nano/microwires were generally formed on a film-like structure mainly consisting of Pb_2O_3 that were preferentially deposited prior to the following ZnO-based products. Additionally, using Sn as the reducing agent, the Zn_2SnO_4 compound formed by ZnO reacted with SnO_2 was deposited at a high temperature (~ 750 °C) on the substrate that was adjacent to the source material (Fig. 1a). In the zone close to the open end of the tube, pure ZnO nano/microstructures were deposited at a lower temperature of 600 °C (Fig. 1b). This is because few Sn and SnO_x diffuse into the zone near the open end of the tube after complete reaction with ZnO. It is suggested that morphologies, sizes, compositions of products, as discussed above, are strongly effected by the used reducing agent, deposition region (temperature and vapor concentration), with/without introducing gas. These parameters are favorable for achieving the controlled growth of ZnO-based nano/microstructures for numerous applications.

Figure 4 shows the PL spectra of the samples fabricated by the sources of ZnO mixed with Sn and deposited in different regions: for a, close to the open side of the tube and for b, near the reaction source. The spectra represent two bands, near band-edge (NBE) emission in the ultraviolet region and broad deep-level emission centered at about
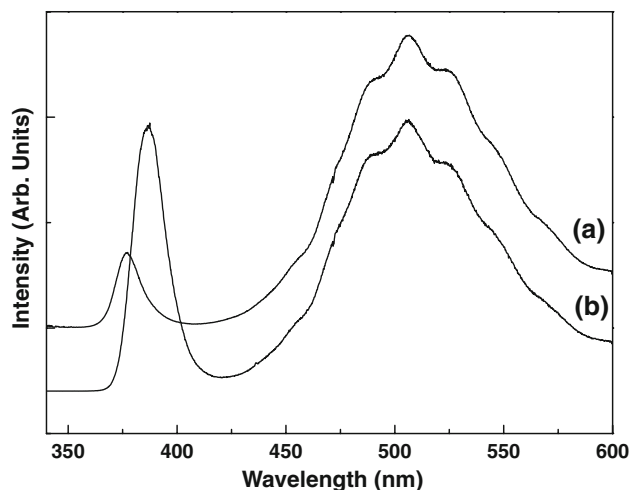
Fig. 4 PL spectra of the samples collected far from (**a**) and near (**b**) the reaction source of ZnO powder mixed with Sn

506 nm. The NBE emission is dominated by excitonic recombination [21], while the deep-level emission is most likely attributed to the recombination luminescence of single-ionized oxygen vacancies [22, 23]. The PL spectra show that the intensity ratio of NBE-related UV to defect-related deep-level emission for b is higher than that of a. It is suggested that the content of Zn_2SnO_4 in the sample formed near the source is favorable to enhance the UV emission. Furthermore, a red shift of the UV emission is found due to the doping-induced band-gap-renormalization (BRG) effect [24, 25]. Except for the two samples, the PL spectra of most products synthesized by the carbon group element reducing agents show broad deep-level emission band and weaker NBE emission (not shown), which can be attributed to the different concentrations of native defects [26] in the samples.
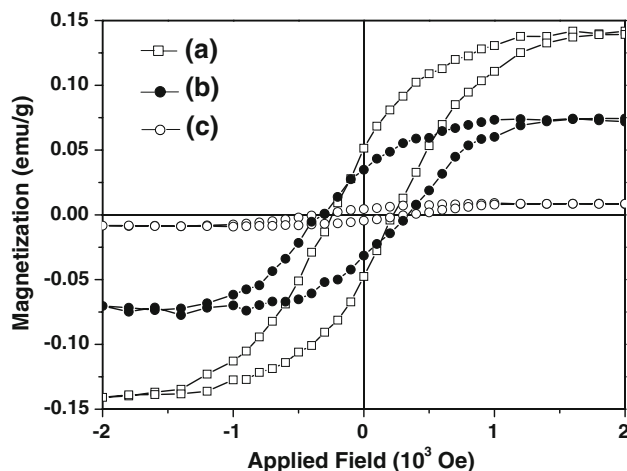
Fig. 5 Magnetization M versus applied magnetic field H for the samples synthesized by the source of ZnO mixed with Pb (**a**), Sn (**b**) and, graphite (**c**)

The magnetization measurements of the selected samples synthesized by the sources of ZnO–Pb (a), ZnO–Sn (b), and ZnO-graphite (c) are shown in the Fig. 5. The samples are RT ferromagnetic. The saturated fields are about 1,740 Oe for sample a (ZnO doped with Pb_2O_3), 1,500 Oe for sample b (ZnO doped with Zn_2SnO_4), and 1,270 Oe for sample c (pure ZnO). The corresponding saturation magnetizations, M_s, are 0.140 emu/g, 0.074 emu/g, and 0.009 emu/g for samples a, b, and c, respectively. It should be pointed out that the M_s of samples a, and b are significantly higher than that of sample c, which might be attributed to the presented impurity phases. It is suggested that these Pb_2O_3 and Zn_2SnO_4 phases would cause the rise of defect and/or oxygen vacancies that result in variation of the ferromagnetic properties of ZnO nano/microstructures [27].

Conclusions

In summary, nano/microsized ZnO have been grown via a thermal evaporation process using ZnO powders mixed with carbon group elements (graphite, Si, Ge, Sn, or Pb). It is noteworthy that the T_{heat} for the cases of Si, Ge, Sn, and Pb is lower than that of graphite due to the smaller ionization energy of the new additional elements. On account of the high vapor pressures of Sn and Pb, the phase of Zn_2SnO_4 or Pb_2O_3 is found in the ZnO nano/microstructures fabricated using ZnO–Sn or ZnO–Pb as the precursor. The RT PL spectral results reveal the doped Zn_2SnO_4 is favorable for increasing the intensity ratio of the NBE-related UV emission to the visible deep-level emission, meanwhile, a redshift appears for the UV emission due to BGR effect. The ZnO nano/microstructures containing some impurities of Pb_2O_3 or Zn_2SnO_4 show RT ferromagnetic with enhanced saturated magnetizations with respect to the case of pure ZnO products.

References

1. M.H. Huang, S. Mao, H. Feick, H. Yan, H. Kind, E. Weber, R. Russo, P. Yang, Science **292**, 1897 (2001)
2. H.D. Li, S.F. Yu, S.P. Lau, E.S.P. Leong, H.Y. Yang, T.P. Chen, A. Abiyasa, C.Y. Ng, Adv. Mater. **18**, 771 (2006)
3. S.K. Marathe, P.M. Koinkar, S.S. Ashtaputre, M.A. More, S.W. Gosavi, D.S. Joag, S.K. Kulkarni, Nanotechnology **17**, 1932 (2006)
4. W.W. Wang, G.M. Zhang, L.G. Yu, X. Bai, Z.X. Zhang, X.Y. Zhao, Physica. E **36**, 86 (2007)
5. M.H. Zhao, Z.L. Wang, C.X. Mao, Nano. Lett. **4**, 587 (2004)
6. H.C. Cheng, C.F. Chen, C.Y. Tsay, Appl. Phys. Lett. **90**, 012113 (2007)
7. M.S. Arnold, P. Avouris, Z.W. Pan, Z.L. Wang, J. Phys. Chem. B **107**, 659 (2003)
8. X.L. Zhu, I. Yuri, X. Gan, I. Suzuki, G.X. Li, Biosens. Bioelectron. **22**, 1600 (2007)
9. C.X. Xu, X.W. Sun, Z.L. Dong, M.B. Yu, Appl. Phys. Lett. **85**, 3878 (2004)
10. B.D. Yao, Y.F. Chan, N. Wang, Appl. Phys. Lett. **81**, 757 (2002)
11. H.D. Li, H. Lv, D.D. Sang, D.M. Li, B. Li, X.Y. Lv, G.T. Zou, Chin. Phys. Lett. **25**, 3794 (2008)
12. S.L. Zhang, Y. Zhang, Z. Fu, S.N. Wu, M. Gao, M. Liu, J. Chen, L. Niu, J.Z. Jiang, Y. Ling, Q. Wang, H. Chen, Appl. Phys. Lett. **89**, 243108 (2006)
13. Y.H. Yang, C.X, Wang, B. Wang, N.S. Xu, G.W. Yang, Chem. Phys. Lett. **403**, 248 (2005)
14. C. Xu, M. Kim, J. Chun, D. Kim, Appl. Phys. Lett. **86**, 133107 (2005)
15. L.S. Wang, X.Z. Zhang, X. Liao, W.G. Yang, Nanotechology **16**, 2928 (2005)
16. R.S. Wagne, W.C. Ellis, Appl. Phys. Lett. **4**, 89 (1964)
17. B.M. Thaddeus, O. Hiroaki, P.R. Subramanian, K. Linda, *Binary Alloy Phase Diagrams* (Materials Park, Ohio, 1990)
18. P.X. Gao, Z.L. Wang, J. Phys. Chem. B **108**, 7534 (2004)
19. P.X. Gao, Z.L. Wang, J. Phys. Chem. B **106**, 12653 (2002)
20. R. Lide David, *CRC Handbook of Chemistry and Physics* (CRC Press, Boca Raton, 2005), p. 4. 128, 129
21. J.X. Duan, X.T. Huang, H. Wang, Q. Zhong, F.L. Sun, X. He, Mater. Chem. Phys. **106**, 181 (2007)
22. Y.Q. Chen, J. Jiang, Z.Y. He, Y. Su, D. Cai, L. Chen, Mater. Lett. **59**, 3280 (2005)
23. K. Vanheusden, W.L. Warren, C.H. Seager, D.R. Tallant, J.A. Voigt, B.E. Gnade, J. Appl. Phy. **79**, 7983 (1996)
24. R. Deng, X.T. Zhang, J. Lumin. **128**, 1442 (2008)
25. J.D. Ye, S.L. Gu, S.M. Zhu, S.M. Liu, Y.D. Zheng, R. Zhang, Y. Shi, H.Q. Yu, Y.D. Ye, J. Cryst. Growth **283**, 279 (2005)
26. A.B. Djurišic', Y.H. Leung, Small **2**, 944 (2006)
27. N.H. Hong, J. Sakai, N. Poirot, V. Brizé, Phys. Rev. B **73**, 132404 (2006)